Anomalous oxygen isotope enrichment in CO_2 produced from O+CO: Estimates based on experimental results and model predictions

Antra Pandey and S. K. Bhattacharya[a)]
Physical Research Laboratory, Navrangpura, Ahmedabad 380 009, India

(Received 19 December 2005; accepted 26 April 2006; published online 15 June 2006)

The oxygen isotope fractionation associated with $O+CO \rightarrow CO_2$ reaction was investigated experimentally where the oxygen atom was derived from ozone or oxygen photolysis. The isotopic composition of the product CO_2 was analyzed by mass spectrometry. A kinetic model was used to calculate the expected CO_2 composition based on available reaction rates and their modifications for isotopic variants of the participating molecules. A comparison of the two (experimental data and model predictions) shows that the product CO_2 is endowed with an anomalous enrichment of heavy oxygen isotopes. The enrichment is similar to that observed earlier in case of O_3 produced by $O+O_2$ reaction and varies from 70‰ to 136‰ for ^{18}O and 41‰ to 83‰ for ^{17}O. Cross plot of $\delta^{17}O$ and $\delta^{18}O$ of CO_2 shows a linear relation with slope of ~0.90 for different experimental configurations. The enrichment observed in CO_2 does not depend on the isotopic composition of the O atom or the sources from which it is produced. A plot of $\Delta(\delta^{17}O)$ versus $\Delta(\delta^{18}O)$ (two enrichments) shows linear correlation with the best fit line having a slope of ~0.8. As in case of ozone, this anomalous enrichment can be explained by invoking the concept of differential randomization/stabilization time scale for two types of intermediate transition complex which forms symmetric ($^{16}O^{12}C^{16}O$) molecule in one case and asymmetric ($^{16}O^{12}C^{18}O$ and $^{16}O^{12}C^{17}O$) molecules in the other. The $\delta^{13}C$ value of CO_2 is also found to be different from that of the initial CO due to the mass dependent fractionation processes that occur in the $O+CO \rightarrow CO_2$ reaction. Negative values of $\Delta(\delta^{13}C)$ (~12.1‰) occur due to the preference of ^{12}C in CO_2^* formation and stabilization. By contrast, at lower pressures (~100 torr) surface induced deactivation makes $\Delta(\delta^{13}C)$ zero or slightly positive. © *2006 American Institute of Physics*. [DOI: 10.1063/1.2206584]

I. INTRODUCTION

The occurrence of anomalous heavy isotope enrichment in ozone has been established by a series of measurements in stratosphere and laboratory. Mauersberger[1] observed that the ozone in stratosphere is enriched in ^{18}O by as much as 400‰ relative to air oxygen. Later, evidence of mass independent enhancement of two heavy isotopologues of ozone ($^{49}O_3$ and $^{50}O_3$) was reported for stratosphere[2,3] as well as in ozone produced in the laboratory.[4–8] Early attempts to explain these anomalous isotope effects lead to the conclusion that symmetry controls the relevant fractionation process. During the last 25 years, several theoretical models have been proposed to explain this anomalous enrichment.[9–23] In recent years, measurement of specific rate coefficients[24–27] of several possible ozone forming channels has brought out the complexities of the isotopic enrichment process. There are surprisingly large differences in the rates of formation of various ozone isotopomers and isotopologues, which suggest that molecular symmetry operates along with many associated quantum restrictions for generating this anomaly. As of now, the underlying microscopic process causing such a large anomalous effect is not clearly resolved though influence from molecular symmetry is suspected to be the principal cause. A phenomenological theory[13–19] has been proposed recently based on a modification of the standard Rice-Ramsperger-Kassel-Marcus (RRKM) model of unimolecular dissociation, which calculates isotopic fractionation in ozone produced by $O+O_2$ recombination reaction under restrictions of symmetry.

The role of symmetry in causing isotopic anomaly can be further constrained if reactions other than $O+O_2$ reaction can be investigated. One such reaction is $O+CO \rightarrow CO_2$, which should also produce a mass independent oxygen isotopic fractionation in the product CO_2 because the relevant isotopic symmetry of O+CO is same as that of $O+O_2$. Carbon being the central atom does not play a direct role in the fractionation of oxygen isotopes. Therefore, the study of $O+CO \rightarrow CO_2$ reaction offers a nice possibility to test the validity of non-RRKM theory of Marcus and his co-workers for nonozone systems.

The O+CO reaction was first studied by Bhattacharya and Thiemens[28,29] (BT) who demonstrated a large mass independent oxygen isotopic enrichment in the product CO_2. However, for several reasons there is a need for further investigation. In the BT experiments, O_2 was dissociated by UV light (in presence of a large reservoir of CO) to generate oxygen atoms, which subsequently react with CO to produce CO_2. They observed a large variation in $\delta^{18}O$ (10‰–60‰) of the product CO_2. The oxygen atoms in CO_2 come from two sources having different isotopic compositions, a well-characterized CO reservoir and an isotopically unknown O

a)Electronic mail: bhatta@prl.res.in

atom reservoir. In BT experiments, presence of UV light allows many parallel reactions to occur with attendant complications. For example, O_2 dissociation produces both $O(^1D)$ and $O(^3P)$. The $O(^1D)$ can undergo an isotopic exchange with CO while quenching and produce isotopically depleted $O(^3P)$ which modifies the original O pool composition. Moreover, UV dissociation of O_2 also produces enriched ozone whose subsequent dissociation generates enriched O atoms. These two sources of $O(^3P)$ introduce complication in determining its composition and the enrichment observed in product CO_2 is therefore difficult to interpret. One of the motivations behind the present experiment was to achieve a better constraint on the O atom composition. In our experiment, ozone with known isotopic composition was photodissociated using visible lamp to produce only $O(^3P)$. Additionally, in BT experiments, as a parallel process, the product CO_2 dissociates at 184.5 and 130 nm, producing lighter oxygen molecules.[30] Thus, the left over CO_2 gets enriched in heavy oxygen isotopes by an uncertain amount. Moreover, to avoid isobaric influence of ^{13}C the product CO_2 was converted to O_2 by reacting it with bromine pentafluoride (BrF_5), which requires somewhat large amount of CO_2; this can introduce uncertainty in the case of small CO_2.

In case of ozone, a short lived excited complex forms during the recombination reaction which transfers its extra energy by collision to the bath gas molecules in order to become a stable molecule. This deactivation collisional stabilization process has a mass dependent fractionation. In case of ozone molecules it is not possible to separate the mass dependent part of total fractionation experimentally. Study of $O+CO \rightarrow CO_2$ reaction gives an opportunity to quantify the mass dependent fractionation that occurs through analysis of carbon isotopes since carbon being the central atom in CO_2 is not affected by the symmetry related part of the fractionation process. The $\delta^{13}C$ of the product CO_2 was measured in the present case.

II. EXPERIMENTAL DETAILS

To investigate the $O+CO \rightarrow CO_2$ recombination reaction, four different sets of experiments were carried out. In sets 1–3 ozone was dissociated by visible light to produce O atoms whereas in set 4, O atom was produced by dissociating pure O_2 with UV light (as in BT). CO was taken directly from a cylinder of high purity. The isotopic composition of tank CO is $\delta^{13}C=-26.6‰$ [relative to CO_2 from Vienna Peedee Belmnite (VPDB-CO_2)], $\delta^{18}O=28.7‰$, $\delta^{17}O=14.9‰$, and of tank O_2 is $\delta^{18}O=24.6‰$ and $\delta^{17}O=12.5‰$. The oxygen isotopic compositions are expressed relative to Vienna standard mean ocean water (VSMOW).

(i) Preparation of ozone by Tesla (set 1: constant O_3 *composition and set 2: variable* O_3 *composition) and by UV (set 3) and photolysis of* (O_3+CO) *mixture*. In sets 1 and 2 experiments, ozone was made by Tesla discharge of oxygen taken in a cylindrical Pyrex reaction chamber (diameter =2.9 cm and volume ~ 70 cc). For all samples of set 1, the discharge conditions (pressure of oxygen, time of discharge, position of LN2 trap, pumping time, and fraction of oxygen converted to ozone) were kept the same to obtain ozone of nearly same composition and amount. The average isotopic composition of O_3 was $\delta^{18}O=27.6‰\pm3.2‰$ and $\delta^{17}O=14.7‰\pm2.3‰$ and average amount of ozone was 89 ± 11 (in μmol O_2) (based on 15 determinations). However, in case of set 2, the conditions were purposely varied and an aliquot was collected in each case for determining the amount and isotopic composition of ozone. In a few cases, samples having $^{18}O/^{16}O$ and $^{17}O/^{16}O$ abundance ratios close to that of the O_2 was made (by converting nearly 100% of O_2 by Tesla discharge). In set 3 samples, ozone was produced in a 5 l chamber fitted with a MgF_2 side window (2 mm thick and 24 mm diameter) by irradiating oxygen at 300 torr with UV light generated by a Hg resonance lamp (184.9 and 253.6 nm) driven by a microwave generator.

The product ozone was frozen by liquid nitrogen (LN_2) and the remaining oxygen pumped away until 2 mtorr pressure (vapor pressure of ozone at LN_2). Keeping the ozone in condensed form in LN_2 temperature, CO was admitted to the reaction chamber (between 7 and 447 torr pressure). Subsequently, the liquid nitrogen trap was removed and the O_3-CO mixture (in room temperature) was photolyzed by visible lamp (a halogen-filled tungsten projection lamp, type Philips 13163, 24 V input, 250 W output power; the emission of the lamp was from 350 to 900 nm) for 30–360 min.

(ii) Photolysis of (O_2+CO) *mixture by UV light (set 4)*. In set 4, approximately 100–400 μmol of O_2 was taken in the 5 l chamber. Subsequently, CO at a pressure of 10–26 torr was taken and the O_2-CO mixture was photolyzed with UV photons from a Hg lamp for 350–1330 min.

(iii) Measurement of $\delta^{18}O$, $\delta^{17}O$ *and* $\delta^{13}C$ *of the product* CO_2. After photolysis, the product CO_2 and left over ozone, if any, were frozen and noncondensable gases (CO and O_2) were pumped out. To separate CO_2 from the left over ozone, the condensed gases were transferred to a chamber containing cleaned nickel foil and heated to 120 °C to decompose any ozone. In most of the experiments, the quantity of O_2 resulting from ozone dissociation on hot nickel surface was not measurable and pumped out. Subsequently, pure CO_2 was collected for isotopic analysis. Control experiments showed that the fractionation produced by hot nickel surface is less than 0.06‰ for $\delta^{45}CO_2$ and 0.1‰ for $\delta^{46}CO_2$ and can be neglected.

To resolve the isobaric effect of ^{13}C in CO_2 of mass 45, the equilibrium exchange method of CO_2 with hot CeO_2 was employed.[31] The sample CO_2 was first analyzed in the mass spectrometer and then transferred to the CeO_2 reaction chamber (kept at 650 °C after flushing it with oxygen gas). After exchange, the CO_2 was collected back and reanalyzed. $\delta^{13}C$, $\delta^{17}O$, and $\delta^{18}O$ values of the product CO_2 were determined from these two sets of δ^{45} and δ^{46} data. A few test runs showed an average yield recovery of ~99% and the change in $\delta^{13}C$ of ~0.02‰. In order to determine blank contribution to product CO_2 coming from reaction of ozone with chamber materials, ozone (~90 μmol) was kept in the same chamber for 8 h without putting CO in it. The isotopic compositions of the blank CO_2 (<5 μmol) were $\delta^{17}O=18.0‰$, $\delta^{18}O=22.5‰$, and $\delta^{13}C=-31.1‰$ and accordingly corrections were made.

TABLE I. Oxygen isotopic composition of CO_2 produced from CO+O reaction for set 1. Ozone was made by Tesla discharge of O_2. Average isotopic composition and amount based on control experiments are $\delta^{18}O=27.6\pm3.2$ and $\delta^{17}O=14.7\pm2.3$ and 89 ± 11, respectively.

Sample No.	Amount of CO (μmol)	Exposure time (min)	Amount of CO_2 produced (μmol)	CO_2 composition		Model prediction		Enrichment	
				$\delta^{18}O$	$\delta^{17}O$	$\delta^{18}O$	$\delta^{17}O$	$\Delta(\delta^{18}O)$	$\Delta(\delta^{17}O)$
A1	1587	50	46	53.6	41.8	−39.6	−20.4	93.2	62.2
A2	1633	50	59	49.9	38.6	−30.3	−16.1	80.2	54.7
A3	1633	150	16	40.8	33.5	−53.7	−23.3	94.6	56.8
A4	1587	240	26	46.0	38.9	−52.3	−25.7	98.3	64.6
A5	1582	210	34	50.3	41.1	−47.3	−23.7	97.6	64.8
A6	1313	30	35	56.3	51.8	−45.7	−23.5	102.0	75.3
A7	1177	40	43	42.4	32.5	−40.0	−21.0	82.4	53.5
A8	1189	100	45	43.0	33.5	−38.3	−20.1	81.3	53.6
A9	1022	330	31	44.5	37.3	−46.1	−24.0	90.6	61.3
A10	67	300	15	59.5	50.2	−38.5	−23.5	98.0	73.7
A11	67	180	12	63.4	52.2	−39.2	−24.1	102.6	76.3
A12	25	180	13	41.5	32.5	−36.7	−22.8	78.2	55.3
A13	1008	180	30	43.8	34.5	−46.1	−24.1	89.9	58.6
A14	1035	180	26	43.8	32.6	−49.0	−25.3	92.8	57.9
A15	46	180	5	56.3	46.3	−39.2	−24.6	95.5	70.9
A16	109	180	7	48.7	39.7	−40.4	−24.5	89.1	64.2

Measurements of carbon and oxygen isotopic compositions of product CO_2 were done using a Europa GEO 20-20 mass spectrometer. Typical error in isotopic measurement of CO_2 was 0.02‰ for both $\delta^{45}CO_2$ and $\delta^{46}CO_2$.

(iv) Measurement of $\delta^{18}O$ *and* $\delta^{17}O$ *of ozone*. For amount and isotopic measurements, ozone was cryogenically transferred to a trap containing molecular sieve (pellet 13X) and converted to oxygen by heating and freezing in succession of two or three times. The error associated with the amount (measured as its oxygen equivalent) measurement is ~0.5%. The oxygen isotopic measurements were done using a VG 903 mass spectrometer with uncertainties of 0.05‰ and 0.2‰ in $\delta^{18}O$ and $\delta^{17}O$, respectively.

III. RESULTS

A. Oxygen isotope fractionation

The results of photolysis experiments pertaining to set 1 are given in Table I and shown in Fig. 1. The cross plot of δ values for CO_2 defines a line with a slope of 0.96±0.07. The maximum $\delta^{18}O$ value observed is 63.4‰ and the corresponding $\delta^{17}O$ value is 52.2 ‰. In most of the cases, $\delta^{17}O$ value of a given CO_2 sample is close to the $\delta^{18}O$. The results for set 2 experiments are given in Table II and the δ values of CO_2 are plotted in Fig. 2. The data points fall on a line with a slope of 0.90±0.04. The highest $\delta^{18}O$ value (113.5‰) is obtained in experiment AC17 where the $\delta^{18}O$ value of the source ozone was also the highest. Additionally, the CO_2 amount was low in this case. We note that if CO amount does not change significantly (for example, in sample numbers AC6, AC7, AC8, and AC9 where the CO amount is ~50 μmol) the δ value of CO_2 increases with that of the ozone. A change of 106‰ in $\delta^{18}O$ value of ozone results in a change of ~87‰ in $\delta^{18}O$ value of CO_2. It is to be noted that in samples AC4, AC15, and AC16, the $\delta^{18}O$ values of CO_2 were low and close to that of CO. In these cases, the ozone had no enrichment as the δ values were close to that of the tank O_2.

The δ values of CO_2 produced in sets 3 and 4 are summarized in Table II and the δ values are plotted against each other in Fig. 3 displaying again a mass independent signature. The average $\delta^{18}O$ and $\delta^{17}O$ values of set 3 CO_2 samples are 74.7‰ and 64.1‰, respectively and for samples of set 4 they are 55.4‰ and 51.9‰. As mentioned before, in sets 3 and 4 two different sources of O atom were used. In set 3, O_3+CO mixture was photolyzed in the presence of visible light whereas in set 4 a mixture of O_2 and CO was photolyzed using UV light from Hg lamp for various time periods.

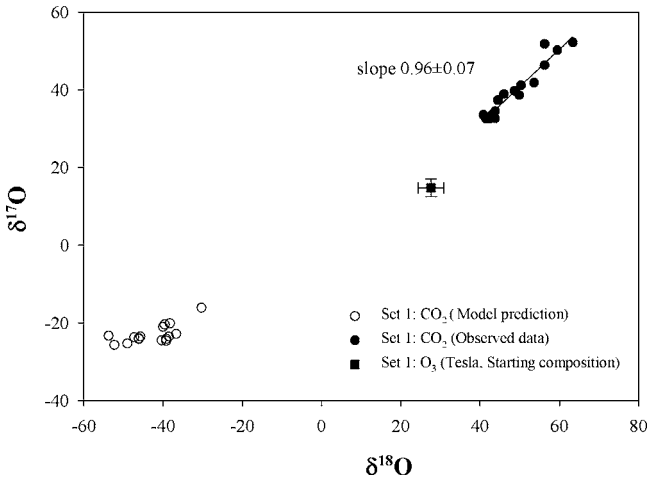

FIG. 1. Oxygen isotopic compositions (in ‰ relative to VSMOW) of product CO_2 (set 1 samples) defining a line with slope of 0.96±0.07. The average $\delta^{18}O$ and $\delta^{17}O$ values of CO_2 samples calculated from the KINTECUS model are −43‰ and −20‰. Note that CO_2 is enriched in heavy oxygen isotopes in an anomalous fashion.

TABLE II. Oxygen isotope ratios of CO_2 produced by reaction O+CO (Sets 2–4).

Sample No.	Amount of Ozone (μmol)	Ozone composition $\delta^{18}O$	Ozone composition $\delta^{17}O$	Amount of CO (μmol)	Exposure time (min)	Amount of CO_2 produced (μmol)	CO_2 composition $\delta^{18}O$	CO_2 composition $\delta^{17}O$	Model prediction $\delta^{18}O$	Model prediction $\delta^{17}O$	Enrichment in CO_2 $\Delta(\delta^{18})$	Enrichment in CO_2 $\Delta(\delta^{17}O)$
						Set 2						
AC1	58	52.7	43.8	129	120	10	40.1	37.2	−30.3	−10.8	70.4	48.0
AC2	62	56.2	46.2	654	150	18	46.0	32.2	−28.3	−9.2	74.3	41.4
AC3	335	56.5	46.2	329	65	104	56.4	47.2	−23.8	−7.6	80.2	54.8
AC4[a]	36	22.1	12.7	309	120	37[b]	26.8	14.6	−41.5	−21.6	68.3	36.2
AC6	68	61.3	50.7	46	60	13	67.0	54.7	−22.4	−6.2	89.4	60.9
AC7	65	55.7	46.8	46	70	6	67.5	54.6	−26.1	−9.1	93.6	63.7
AC8	71	101.9	89.1	46	115	11	97.5	88.5	−1.4	14.7	98.9	73.8
AC9	76	36.3	25.7	46	135	⋯	46.4	38.9	−34.2	−18.7	80.6	57.6
AC10	68	38.3	28.1	1269	140	30	50.9	42.2	−40.1	−16.9	91.0	59.1
AC11	74	62.6	48.8	1269	150	28	67.5	56.8	−36.9	−12.1	104.4	68.9
AC12	48	89.6	70.3	170	120	14	88.0	71.6	−12.7	1.9	100.7	69.7
AC13	89	60.4	46.7	1353	65	36	64.0	54.9	−34.8	−11.8	98.8	66.7
AC14	47	88.9	69.0	1212	180	24	83.3	69.7	−23.3	−2.3	106.6	72.0
AC15[a]	97	24.3	11.7	386	115	30	29.7	21.1	−41.8	−24.4	71.5	45.5
AC16[a]	91	23.1	11.1	386	125	11	31.8	18.6	−47.7	−27.6	79.5	46.2
AC17	68	128.1	101.8	88	180	9	113.5	90.8	10.4	19.1	103.1	71.7
						Set 3[c]						
AS1	80	128.7	101.8	3889	180	13	84.7	70.2	−43.7	−6.6	128.4	76.8
AS2				5834	90	10	74.9	64.9	−55.4	−12.4	130.3	77.3
AS3				5834	360	12	71.9	63.4	−53.8	−11.6	125.7	75.0
AS4				5834	90	9	70.2	54.6	−55.4	−12.4	125.6	67.0
AS5				7778	90	26	71.8	67.5	−52.1	−10.6	123.9	78.1
						Set 4[d]						
AB1		24.6	12.5	4521	355	7	53.6	48.2	−70.3	−22.6	123.9	70.8
AB2		(O_2)		4589	610	10	51.3	48.4	−73.7	−23.8	125.0	72.2
AB3				7013	1330	21	59.5	57.0	−76.1	−24.7	135.6	81.7
AB4				7013	550	18	57.1	53.8	−70.7	−29.0	127.8	82.8

[a]Ozone with nearly no enrichment (~100% of oxygen was converted into ozone) in heavy oxygen isotopes was used for the reaction.
[b]CO_2 amount is unexpectedly high for unknown reason.
[c]Ozone was made from UV dissociation of O_2. Repeat experiments show ~1‰ variation in $\delta^{18}O$ and $\delta^{17}O$ of ozone and ~7 μmol variation in its amount. Average ozone amount used for the reaction was ~81 μmol.
[d]O_2 and CO mixture was photolysed with light from UV lamp.

B. Carbon isotope fractionation

It is interesting to note the nature of pressure variation of $\delta^{13}C$ of CO_2 (relative to the starting CO composition and defined by $\Delta\delta^{13}C = \delta^{13}C\ (CO_2) - \delta^{13}C(CO)$). $\Delta\delta^{13}C$ and CO pressure for all the four sets are listed in Table III and plotted against each other in Fig. 4. $\Delta(\delta^{13}C)$ vary from +3.8‰ to −14.6‰. At high CO pressure (between 270 and 445 torr), the average value is −12.1‰. With CO pressure below 270 torr $\Delta(\delta^{13}C)$ tends to increase with decrease in pressure becoming positive at very low pressures. The most positive value of $\Delta\delta^{13}C$=3.8‰ is obtained at 18 torr (sample A10).

IV. DISCUSSION

A. Model simulation

A commercially available software program, KINTECUS (WINDOWS version 3.8, 2005) developed by Ianni,[32] Vast Technologies Development (www.kintecus.com), was utilized to simulate the experimental conditions for interpreting

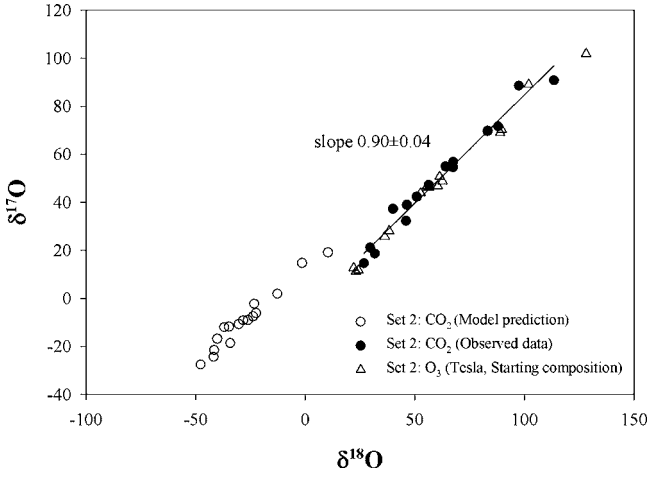

FIG. 2. Oxygen isotopic compositions of CO_2 samples from set 2. The best-fit line relating $\delta^{17}O$ with $\delta^{18}O$ gives a slope of 0.90±0.04 suggesting anomalous enrichments in heavy oxygen isotopes. Ozone compositions used in these experiments are also shown in the plot. The average isotopic composition of CO_2 samples as predicted by the KINTECUS model is $\delta^{18}O$=−27.2‰ and $\delta^{17}O$=−8.9‰. The maximum enrichment seen in this set is 106.6‰ and 72.0‰ in $\delta^{18}O$ and $\delta^{17}O$, respectively, corresponding to ozone compositions of 89‰ and 69‰ in $\delta^{18}O$ and $\delta^{17}O$, respectively.

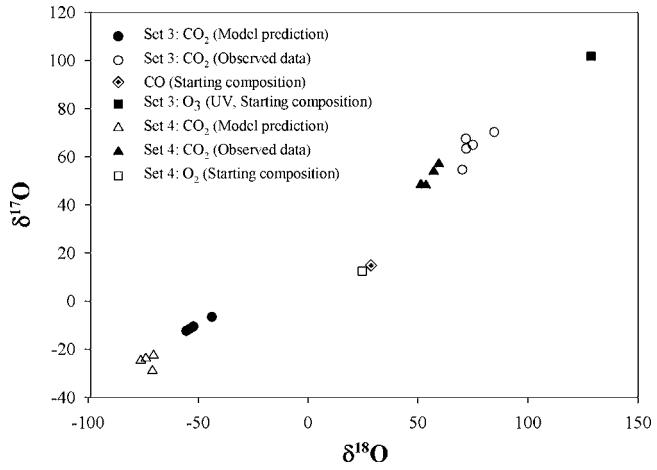

FIG. 3. A three-isotope plot of the experimental data observed in sets 3 and 4 along with results of model simulation. In set 3, O_3–CO mixture was photolyzed using visible lamp whereas in set 4, O_2–CO mixture was photolysed in UV light. The average $\delta^{18}O$ and $\delta^{17}O$ enrichments (difference between observed data and model prediction) are (126.8, 74.8) in set 3 and (128.1, 76.9) in set 4.

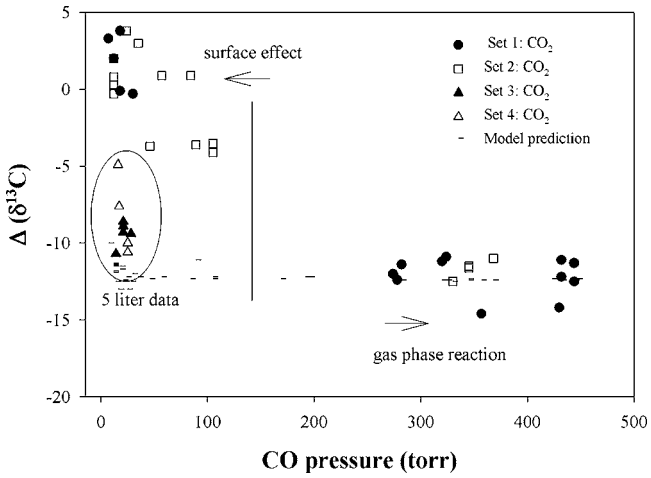

FIG. 4. Difference between $\delta^{13}C$ value of the product CO_2 and the $\delta^{13}C$ value of initial CO ($\Delta\delta^{13}C$)=$\delta^{13}C(CO_2)-\delta^{13}C$ (CO) plotted against CO pressure. In sets 1 and 2, between 270 and 445 torr the average $\Delta\delta^{13}C$ value is −12.1‰, which is close to the expected value (discussed in the text). The pattern suggests a surface effect at lower pressures. In sets 3 and 4, experiments were carried out in a 5 l chamber where the surface effect is smaller due to lower surface/volume ratio.

TABLE III. Change in $\delta^{13}C$ value of product CO_2 relative to the initial CO. $\Delta(\delta^{13}C)$ ($\Delta(\delta^{13}C)$ is defined as $[\delta^{13}C(\text{product or model } CO_2)-\delta^{3}C(\text{initial CO})]$). is calculated for observed CO_2 and also using model predicted $\delta^{13}C$ value of CO_2. Corresponding CO pressures are also shown. A depletion of 4.3% is to be added to model value to account for CO_2^* stabilization.

Sample No.	CO pressure (torr)	Observed $\Delta(\delta^{13}C)$ (‰)	Model result $\Delta(\delta^{13}C)$ (‰)	Sample No.	CO pressure (torr)	Observed $\Delta(\delta^{13}C)$ (‰)	Model result $\Delta(\delta^{13}C)$ (‰)
	Set 1[a]				Set 2[b]		
A1	432	−11.1	−8.1	AC1	35	3.0	−7.9
A2	444	−11.3	−8.1	AC2	57	0.9	−7.9
A3	444	−12.5	−8.1	AC3	89	−3.6	−6.8
A4	432	−12.2	−8.1	AC4	84	0.9	−8.0
A5	430	−14.2	−8.1	AC6	12	0.3	−7.0
A6	357	−14.6	−8.1	AC7	12	−0.3	−7.6
A7	320	−11.2	−8.1	AC8	12	2.0	−7.2
A8	324	−10.9	−8.1	AC9	12	0.8	−7.1
A9	278	−12.4	−8.1	AC10	345	−11.6	−8.1
A10	18	3.8	−7.2	AC11	345	−11.5	−8.1
A11	18	−0.1	−7.4	AC12	46	−3.7	−8.0
A12	7	3.3	−5.7	AC13	368	−11.0	−8.1
A13	274	−12.0	−8.1	AC14	330	−12.5	−8.2
A14	282	−11.4	−8.1	AC15	105	−4.1	−7.9
A15	12	2.0	−7.5	AC16	105	−3.5	−8.0
A16	30	−0.3	−7.7	AC17	24	3.8	−7.9
	Set 3[c]				Set 4[d]		
AS1	14	−10.7	−8.2	AB1	16	−4.9	−8.7
AS2	21	−8.9	−8.1	AB2	17	−7.6	−8.7
AS3	21	−9.3	−8.1	AB3	25	−10.6	−8.7
AS4	21	−8.6	−8.1	AB4	25	−10.0	−8.7
AS5	28	−9.4	−8.2				

[a]O_3 (constant composition) and CO mixture was photolyzed by visible light in 70 cc chamber.
[b]O_3 (variable composition) and CO mixture was photolyzed in 70 cc chamber.
[c]Photolysis of O_3–CO mixture in 5 1 chamber.
[d]O_2–CO mixture was photolyzed by UV light in 5 1 chamber.

the laboratory data. The approach to use this model is described below.

(i) Performance test of the KINTECUS *model in case of ozone dissociation: Determination of ozone dissociation rate constant (k_1).* The process of ozone dissociation has been studied earlier by many workers including our own group[33] and this was used as a test case. Two additional motivations prompted this. First, we needed to determine the ozone dissociation rate constant that should be used in our experimental configuration as it depends on the integration of the product of flux of photons at a given λ and corresponding cross section of absorption over the wavelength range given by the tungsten lamp. This parameter was estimated by comparing the total amount of O_2 produced (when a given amount of ozone with known isotopic composition was photolyzed by the same lamp in the same chamber) with the value predicted by the model. After photolysis, the isotopic composition and amount of product oxygen and left over ozone were measured.

(ii) Input parameters for model in ozone dissociation by visible light. The KINTECUS model was used by incorporating all the basic reactions as well as isotopic exchange reactions involving isotopes and isotopomers of O, O_2, and O_3 are summarized in Table IV (reaction sets 1–4). For convenience, the following notations were used: $O=^{16}O$, $Q=^{18}O$, and $P=^{17}O$. To simplify the calculations, multiply substituted species (OQP, QQQ, QQP) having very small abundances were not included. The rate constants were obtained mostly from Anderson *et al.*,[34] DeMore *et al.*,[35] Janssen *et al.*,[27] and some were calculated based on the collision correction. Delta for a given heavy isotope in a molecular species is defined relative to VSMOW by calculating the ratio of the total concentration of that isotopomer (singly substituted species only) to the total light isotope concentration considering all the isotopomers of that molecule.

We assume that during ozone photolysis the O atom is derived *only* from the base position.[36] An important issue, therefore, is how to obtain the isotopic composition of the base atoms since composition of the base atom relative to the total ozone is not known *a priori* for all enrichment levels. When ozone is highly enriched (40‰ or above) abundances of asymmetric ozone species are calculated using the formula given by Janssen[37] relating enrichment (in ^{18}O) in asymmetric species, E^{50} (relative to its statistical abundance) with enrichment in total ozone: E^{50} (asymmetric) $=-1.7+1.33\times E^{50}$ (total) $-0.0038\times(E^{50})^2$, otherwise asymmetric abundance was taken to be same as that of initial ozone. The same relation is assumed for calculating enrichment E^{49} (asymmetric).

It is relatively more difficult to break $O-Q$ and $O-P$ bond than the $O-O$ bond since their bond energies are slightly higher. Therefore, dissociation rates for $O-Q$ and $O-P$ bond are lower by 0.972 and 0.988 compared to $O-O$ bond.[38] Note the factor 0.5 for rate constants in reactions involving two product channels. For the isotopic exchange reaction (reaction set R2) between Q and OO, the forward exchange rate k_8 was taken from Anderson *et al.*[34] The equilibrium constant K_{eq} for this reaction was calculated using rigid rotor harmonic oscillator approximation (following Kaye and Strobel[9]) and the backward exchange rate was obtained. k_{11} was calculated in a similar way. For ozone formation reaction (R3), most of the rate constants were taken from the recent experimental data of Janssen *et al.*[27] Additional factor of 0.5 is applied to account for the symmetry number for obtaining each rate coefficient. The reaction set R4 describes a secondary channel of ozone dissociation by its collision with O atom.

Plugging in the initial ozone concentration and the photolysis time as input parameters the dissociation rate in the model was adjusted to get the observed amounts of product oxygen and left over ozone. We obtained a value of 2.5×10^{-3} as the best estimate for k_1.

To obtain the isotope ratios, the KINTECUS model was run to simulate the ozone dissociation process after plugging in the initial ozone concentration and isotopic composition with $k_1=2.5\times10^{-3}$. The experimental values of $\delta^{18}O$ and $\delta^{17}O$ of the product O_2 (−12.4, −4.3) and the left over ozone (7.9, 6.7) agree well with the model prediction, O_2: (−10.6, −3.0) and O_3: (7.5, 6.3). This agreement provides a well-constrained value of k_1 and indicates that the model is suitable for estimating the isotopic fractionations properly. The model predicts amount and oxygen isotopic composition with an accuracy of 1 μmol and ±1.5‰, respectively.

(iii) Input parameters for visible light dissociation of ozone in (O_3+CO) *mixture (sets 1–3).* Reaction sets R1–R6 (Table IV) were included in the model. For convenience, $C=^{12}C$, $D=^{13}C$, and we neglect multiply substituted species. For isotopic exchange reaction between O and CO the backward reaction rate k_{29} and k_{31} was obtained from the forward reaction rate[39] k_{28} and the equilibrium constant by considering a rigid rotor harmonic oscillator approximation.

Slanger *et al.*[40] showed O+CO recombination rate to be dependent on the characteristics of the third body (M) and found the rate constants to be $(2.3\pm0.4)\times10^{-36}$, $(3.9\pm0.7)\times10^{-36}$, and $(6.2\pm0.9)\times10^{-36}$ for $M=N_2$, CO, and CO_2 whereas Yung and DeMore[41] reported 4.3×10^{-36} and 1.1×10^{-35} for $M=$CO and CO_2, respectively. This is because polyatomic molecules as a third body can take away the excess energy from CO_2^* more efficiently and enhance the stabilization rate. In our case, the rate constant k_{32} was taken to be 4.3×10^{-36}. However, this yields much lower amount of product CO_2 compared to what we obtained experimentally. We are not sure of the exact reason but suspect that the assumed reaction rate may not be valid where M represents mixed gases such as CO, O_2, and O_3. Additionally, surface induced stabilization might have played a role. Since the KINTECUS model considers an infinite volume reaction cell, to get the model CO_2 amount close to that observed, the total concentration of all the molecules $[M]$ in the chamber was enhanced by a suitable factor f determined separately in each case. A plot of f against CO pressure (Fig. 5) shows that f increases with decrease in pressure. This is quite expected

TABLE IV. List of various gas phase reactions along with the rate constants used in the kinetic model (KINTECUS) for simulation of products from O_3+CO photolysis by visible light.

	Reactions[a]	Rate coefficient[b]	References
	R1 (ozone photolysis)		
R(1*O*)	$OOO+h\nu \rightarrow O+OO$	$k_1=2.5\times10^{-3}$	(See text)
R(1*Q*a)	$OOQ+h\nu \rightarrow O+OQ$	$k_2=0.5\times k_1$	
R(1*Q*b)	$OOQ+h\nu \rightarrow Q+OO$	$k_3=0.5\times0.972\times k_1$	38
R(1*Q*c)	$OQO+h\nu \rightarrow O+OQ$	$k_4=0.972\times k_1$	
R(1*P*a)	$OOP+h\nu \rightarrow O+OP$	$k_5=0.5\times k_1$	
R(1*P*b)	$OOP+h\nu \rightarrow P+OO$	$k_6=0.5\times0.988\times k_1$	38
R(1*P*c)	$OPO+h\nu \rightarrow O+OP$	$k_7=0.988\times k_1$	
	R2 (Isotopic exchange of O atom with oxygen)		
R(2*Q*a)	$Q+OO \rightarrow O+OQ$	$k_8=2.90\times10^{-12}$	34
R(2*Q*b)	$O+OQ \rightarrow Q+OO$	$k_9=1.34\times10^{-12}$	
R(2*P*a)	$P+OO \rightarrow O+OP$	$k_{10}=2.90\times10^{-12}$	
R(2*P*b)	$O+OP \rightarrow P+OO$	$k_{11}=1.39\times10^{-12}$	
	R3 (ozone formation)		
R(3*O*)	$O+OO+M \rightarrow OOO+M$	$k_{12}=6.0\times10^{-34}$	27
R(3*Q*a)	$O+OQ+M \rightarrow OOQ+M$	$k_{13}=0.5\times1.45\times k_{12}$	
R(3*Q*b)	$O+OQ+M \rightarrow OQO+M$	$k_{14}=0.5\times1.08\times k_{12}$	
R(3*Q*c)	$Q+OO+M \rightarrow OOQ+M$	$k_{15}=0.92\times k_{12}$	
R(3*Q*d)	$Q+OO+M \rightarrow OQO+M$	$k_{16}=0.006\times k_{12}$	
R(3*P*a)	$O+OP+M \rightarrow OOP+M$	$k_{17}=0.5\times1.32\times k_{12}$	
R(3*P*b)	$O+OP+M \rightarrow OPO+M$	$k_{18}=0.5\times1.04\times k_{12}$	
R(3*P*c)	$P+OO+M \rightarrow OOP+M$	$k_{19}=1.03\times k_{12}$	
R(3*P*d)	$P+OO+M \rightarrow OPO+M$	$k_{20}=0.006\times K_{12}$	
	R4 (ozone decomposition)		
R(4*O*)	$OOO+O \rightarrow OO+OO$	$k_{21}=8.0\times10^{-15}$	35
R(4*Q*a)	$OOO+Q \rightarrow OO+OQ$	$k_{22}=0.957\times k_{21}$	
R(4*Q*b)	$OOQ+O \rightarrow OO+OQ$	$k_{23}=0.995\times k_{21}$	
R(4*Q*c)	$OQO+O \rightarrow OQ+OO$	$k_{24}=0.995\times k_{21}$	
R(4*P*a)	$OOO+P \rightarrow OO+OP$	$k_{25}=0.978\times k_{21}$	
R(4*P*b)	$OOP+O \rightarrow OO+OP$	$k_{26}=0.997\times k_{21}$	
R(4*P*c)	$OPO+O \rightarrow OP+OO$	$k_{27}=0.997\times k_{21}$	
	R5 (Isotopic exchange of O atom with CO)		
R(5*Q*a)	$Q+CO \rightarrow O+CQ$	$k_{28}=8.3\times10^{-16}$	39
R(5*Q*b)	$O+CQ \rightarrow Q+CO$	$k_{29}=6.9\times10^{-16}$	
R(5*P*a)	$P+CO \rightarrow O+CP$	$k_{30}=8.3\times10^{-16}$	
R(5*P*b)	$O+CP \rightarrow P+CO$	$k_{31}=7.9\times10^{-16}$	
	R6 (CO_2 formation)		
R(6*O*)	$O+CO+M \rightarrow COO+M$	$k_{32}=4.3\times10^{-36}$	40
R(6O^-)	$O+DO+M \rightarrow DOO+M$	$k_{33}=0.994\times k_{32}$	
R(6*Q*a)	$O+CQ+M \rightarrow COQ+M$	$k_{34}=0.988\times k_{32}$	
R(6*Q*b)	$Q+CO+M \rightarrow COQ+M$	$k_{35}=0.964\times k_{32}$	
R(6*P*a)	$O+CP+M \rightarrow COP+M$	$k_{36}=0.994\times k_{32}$	
R(6*P*b)	$P+CO+M \rightarrow COP+M$	$k_{37}=0.981\times k_{32}$	

[a]Reaction sets R1–R4 were included in ozone dissociation model whereas for experiments involving photolysis of (O_3+CO) mixture by visible light all the reaction sets (R1–R6) were considered.
[b]Units for two-body and three-body rate coefficients are $cm^3\ s^{-1}$ and $cm^6\ s^{-1}$, respectively, *O*, *P*, *Q*, *C*, and *D* denote ^{16}O, ^{17}O, ^{18}O, ^{12}C, and ^{13}C, respectively.

because surface mediated stabilization reactions should dominate at lower pressures. Enhancing $[M]$ by this way increases the amount of CO_2 produced but it also has effect on $\delta^{18}O$ and $\delta^{17}O$ values (higher f results in higher δ values; Table V) though not on $\delta^{13}C$. The average change in $\delta^{18}O$ is ~8‰ except in two cases where the values are high (~22‰ and 28‰). For further interpretation we take f values to be as determined in each case.

(iv) Input parameters for UV dissociation of (O_2+CO) *mixture (set 4).* In this case, in addition to those in Table IV, six more reaction sets (R1–R6 of Table VI) describing the production of singlet and triplet atoms and their quenching to ground state were considered. The O_2 and O_3 photolysis rate constants were calculated from the available photochemical cross-section data[35] and known photon flux ~1 $\times10^{15}$ photons $cm^{-2}\ s^{-1}$ of the Hg lamp. Earlier studies[35,42]

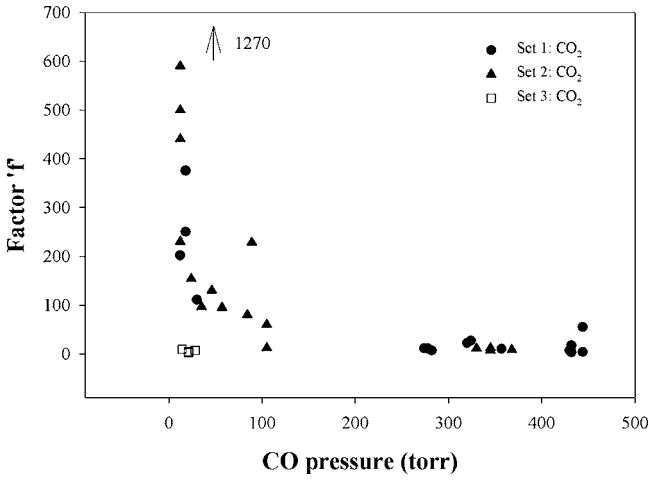

FIG. 5. Variation of factor f (which enhances CO_2 production by increasing $[M]$) with pressure. f increases with decrease in CO pressure suggesting increased importance of surface induced stabilization of CO_2^*. For high CO pressure or experiments done in 5 l chamber, f ranges from 1 to 55 whereas for low CO amount, value of f could be as high as ~1270.

showed that during ozone photolysis in UV light, production of singlet species ($O(^1D)$, $O_2(^1\Delta)$) takes place in 90% cases whereas only in 10% cases triplet products form. Therefore, rate constants of reaction sets 2 and 3 are multiplied by factor of 0.9 and 0.1, respectively.

B. Model results

(i) Oxygen isotope enrichment. The oxygen isotopic compositions (in ‰ relative to VSMOW) of CO_2 predicted by the simulation model corresponding to various sets are summarized in Tables I and II and plotted against each other in Figs. 1–3. The $\delta^{18}O$ values vary from −53.7 to −30.3 (set 1), −47.7 to 10.4 (set 2), −55.4 to −43.7 (set 3), and −76.1 to −70.3 (set 4); corresponding variations in $\delta^{17}O$ values are from −25.7 to −16.1, −27.6 to 19.1, −12.4 to −6.6, and −29.0 to −22.6, respectively. For further discussion, we define the enrichment as $\Delta(\delta^{18}O)=\delta^{18}O_{observed}-\delta^{18}O_{model}$ and same for $\Delta(\delta^{17}O)$. The average enrichment values (in $^{18}O/^{16}O$ corresponding to the four sets are 91.6, 88.2, 126.8, and 128.1; the respective enrichments in $^{17}O/^{16}O$ are 62.7, 58.5, 74.8, and 76.9. The maximum CO_2 enrichment occurs in sets 3 and 4. It is interesting to note that enrichments of sets 3 and 4 samples are similar even though the O atom sources were different. Apparently, it does not matter whether the O atom is produced by visible light dissociation of O_3 or UV light dissociation of O_2. This must be due to the fast isotopic exchange between $O-O_2$ and O–CO, which changes the isotopic composition of O atom significantly before it recombines with CO to produce CO_2. Due to fast exchange, the O atom looses memory of its source and initial composition.

Enrichment in CO_2 shows a weak correlation with the amount of product CO_2. In cases where the product CO_2 amount was relatively less enrichments in ^{18}O and ^{17}O were higher.

(ii) Carbon isotope fractionation. The average value of $\Delta(\delta^{13}C)$ (defined as change in $\delta^{13}C$ of the product CO_2 relative to the initial CO) predicted by the model is −8.1‰ (see Table III) and is constant for all samples, whereas the observed $\Delta(\delta^{13}C)$ value varies from −14.6‰ to +3.8‰. We note that carbon isotope fractionation in the gas phase recombination reaction $O+CO\rightarrow CO_2$ is a combination of two mass dependent fractionation processes arising due to collision. During O+CO recombination forming CO_2^*, lighter CO isotopologues collide with O at slightly higher rates due to lower reduced mass of the colliding pair. $^{13}C^{16}O$ collides with ^{16}O atoms at a rate of 0.994 of the collision rate of $^{12}C^{16}O$. Consequently CO_2^* is depleted in heavy carbon isotope by 6.3‰. After its formation, CO_2^* undergoes various activation and deactivation collisions and transfers its extra energy to the bath gas molecules in discrete steps of ΔE per collision. The ratio of the collision rates for the colliding pairs, $^{16}O^{13}C^{16}O-^{12}C^{16}O$ and $^{16}O^{12}C^{16}O-^{12}C^{16}O$ is 0.996 resulting in 4.3‰ depletion in ^{13}C of CO_2. Therefore, the formation and stabilization of CO_2^* in gas phase are expected to be associated with 10.6‰ depletion of ^{13}C in the product CO_2. The observed average value of $\Delta\delta^{13}C$ in the pressure range of 270–445 torr is −12.1‰, which is close to this calculated value. Since the CO_2^* collisional stabilization process is not included in the model, it predicts a lower magnitude of $\Delta(\delta^{13}C)$ (~−8.1‰).

To explain the positive $\Delta\delta^{13}C$ value (in sets 1 and 2) at low pressure we invoke the concept of surface mediated stabilization mechanism that is expected to occur at lower pressures. Surface-induced stabilization helps the activated complex to loose its extra kinetic energy quite efficiently and become a stable molecule. We postulate that the activated complex CO_2^* has a long-range weak interaction with a reactive atom of the surface forming a transient bond. The amount of energy released from the activated complex is absorbed as vibrations of the lattice and dissipated as heat from the surface. The complex remains on the surface for a short time determined by its sticking coefficient and vibrates in a shallow potential well. The process can be written as $CO_2^*+W\rightarrow(CO_2^*\cdots W)\rightarrow CO_2+W$. In a surface induced stabilization process, transfer of excess energy depends mainly on the sticking coefficient of the molecule. A recent study[43] has shown that sticking coefficient is higher for heavier isotopomers due to their lower zero point energy. Therefore, $^{13}CO_2^*$ is expected to have a larger sticking coefficient and therefore, more chance to form stable molecule. It is not clear as to how much enrichment occurs due to this process but a value of ~10‰ would account for the maximum observed value of ~3.8‰ after canceling the offset of −6.3‰ (due to O and CO collisions in gas phase as explained above). In a range of 50–110 torr, $\Delta\delta^{13}C$ have positive as well as negative values and show large variation from −4.1‰ to +0.9‰. This could be due to competitive influence of surface induced stabilization and deactivating collisional stabilization the former having temperature dependence. The role of surface is supported by comparison of sets 3 and 4 data with sets 1 and 2 data, e.g., for samples AS1 (set 3) and A15 (set 1), AC6, AC7, AC8, and AC9 (set 2). All these experiments were done at the same pressure (12–14 torr),

TABLE V. Effect of factor f on the predicted oxygen isotopic composition of the product CO_2. Model A is for $f=1$. In model B, $[M]$ was enhanced by f to reproduce the observed amount of CO_2. The average difference between the two predictions is ~8‰.

Sample No.	CO_2 amount (μmol) (obs.)	Model A			Model B			Difference A−B
		f	Amount (μmol)	$\delta^{18}O$	f	Amount (μmol)	$\delta^{18}O$	
				Set 1				
A1	46.0	1	11.5	−58.2	16.8	45.9	−39.6	−18.6
A2	59.3		12.0	−58.4	55.0	54.1	−30.3	−28.1
A3	15.9		9.8	−62.8	3.5	16.3	−53.7	−9.0
A4	25.5		13.9	−57.6	3.3	26.9	−52.3	−5.2
A5	33.7		13.8	−57.6	6.8	35.9	−47.3	−10.3
A6	34.8		7.5	−57.7	10.2	34.3	−45.7	−12.0
A7	42.9		7.0	−56.8	22.0	42.4	−40.0	−16.8
A8	44.6		8.8	−56.3	27.0	45.1	−38.3	−18.1
A9	30.7		7.9	−55.1	10.8	30.9	−46.1	−9.0
A10	14.5		0.1	−38.9	375.0	15.0	−38.5	−0.4
A11	12.2		0.1	−39.4	250.0	11.8	−39.2	−0.2
A12	13.0		0.03	−37.3	1270.0	11.9	−36.7	−0.7
A13	30.3		7.5	−55.1	10.9	30.7	−46.1	−9.0
A14	26.1		7.8	−55.3	6.6	25.1	−49.0	−6.3
A15	4.9		0.07	−38.4	202.0	6.9	−39.2	0.8
A16	7.3		0.2	−41.0	111.0	11.6	−40.4	−0.6
				Set 2				
AC1	9.6	1	0.3	−32.7	96.5	10.2	−30.3	−2.4
AC2	17.7		0.6	−34.5	95.0	17.1	−28.3	−6.2
AC3	104.1		1.4	−31.6	228.0	106.0	−23.8	−7.8
AC4	37.0		9.7	−55.0	80.0	15.2	−41.5	−13.6
AC6	12.8		0.05	−23.7	590.0	11.4	−22.4	−1.3
AC7	6.3		0.05	−26.1	230.0	6.0	−26.1	0.0
AC8	11.3		0.06	−0.5	500.0	10.7	−1.4	0.9
AC9	···		0.06	−34.4	440.0	10.3	−34.2	−0.2
AC10	30.0		9.3	−55.5	12.0	30.9	−40.1	−15.3
AC11	27.9		9.6	−47.9	6.6	26.9	−36.9	−11.1
AC12	14.3		0.4	−20.4	130.0	14.1	−12.7	−7.7
AC13	35.6		9.8	−47.4	8.5	34.7	−34.8	−12.6
AC14	23.7		7.8	−45.4	10.9	22.6	−23.3	−22.1
AC15	30.4		1.6	−49.2	60.0	30.5	−41.8	−7.4
AC16	11.3		1.6	−50.0	12.0	12.1	−47.7	−2.3
AC17	9.0		0.15	11.1	154	9.8	10.4	0.7
				Set 3				
AS1	13.6	1	2.4	−53.1	9.4	12.8	−43.7	−9.4
AS2	10.0		4.4	−59.2	2.8	9.6	−55.4	−3.7
AS3	12.0		4.5	−59.3	3.9	12.1	−53.8	−5.5
AS4	8.9		4.4	−58.6	2.8	9.6	−55.4	−3.1
AS5	25.9		6.8	−62.7	7.5	26.1	−52.1	−10.6

but they show large difference in $\Delta\delta^{13}C$ value (−10.7‰–2.0‰, respectively). AS1 experiment was done in the 5 l chamber, which minimized the role of surface during the recombination process resulting in negative $\Delta\delta^{13}C$ value. It is noted that there is no anomalous enrichment in carbon isotope since carbon being the central atom in CO_2 molecule is not affected by the symmetry related part of the total fractionation process.

There is considerable difference (40‰–50‰) between the enrichments observed in $^{18}O/^{16}O$ and $^{17}O/^{16}O$ ratios of CO_2 produced in 70 cc reaction vessel (sets 1 and 2) and in 5 l reaction chamber (sets 3 and 4). The exact reason for this difference is not clear but part of it could be due to the effect of surface. The surface effect can be seen clearly from the oxygen isotopic composition of CO_2 in samples AS1 and AC17. Both the experiments were done at low pressure with nearly the same ozone composition. In AS1 (5 l) the isotopic composition of CO_2 is less by 28.8‰ in ^{18}O than that of AC17. We also note that AS1 sample has lower $\Delta\delta^{13}C$ value (by 14.5‰). Assuming that surface induced stabilization is essentially a mass dependent effect, a lower $\delta^{13}C$ value by 14.5‰ would imply lower $\delta^{18}O$ value by 29.0‰, which is

TABLE VI. List of reactions included in the KINTECUS model for simulating the photolysis reaction of (O_2+CO) mixture using UV light (set 4 and Bhattacharya-Thiemens data). Fractionation factors 0.983 (for *Q* species) and 0.989 (for *P* species) are taken from Chakraborty and Bhattacharya (Ref. 33).

	Reactions	Rate coefficient
R1 (oxygen photolysis)		
R(1A)	$OO+h\nu \rightarrow O+O$	$k_1=8.7\times10^{-7}$
R(1B)	$OQ+h\nu \rightarrow O+Q$	$k_2=0.983\times k_1$
R(1C)	$OP+h\nu \rightarrow O+P$	$k_3=0.989\times k_1$
R2 (ozone photolysis: singlet Products)		
R(2A)	$OOO+h\nu \rightarrow O(^1D)+OO(^1\Delta)$	$k_4=0.9(1\times10^{-2})$
R(2B)	$OOQ+h\nu \rightarrow O(^1D)+OQ(^1\Delta)$	$k_5=0.5\times k_4$
R(2C)	$OOQ+h\nu \rightarrow Q(^1D)+OO(^1\Delta)$	$k_6=0.5\times0.983\times k_4$
R(2D)	$OQO+h\nu \rightarrow O(^1D)+OQ(^1\Delta)$	$k_7=0.983\times k_4$
R(2E)	$OOP+h\nu \rightarrow O(^1D)+OP(^1\Delta)$	$k_8=0.5\times k_4$
R(2F)	$OOP+h\nu \rightarrow P(^1D)+OO(^1\Delta)$	$k_9=0.5\times0.989\times k_4$
R(2G)	$OPO+h\nu \rightarrow O(^1D)+OP(^1\Delta)$	$k_{10}=0.989\times k_4$
R3 (ozone photolysis: triplet Products)		
R(3A)	$OOO+h\nu \rightarrow O+OO$	$k_{11}=0.1(1\times10^{-2})$
R(3B)	$OOQ+h\nu \rightarrow O+OQ$	$k_{12}=0.5\times k_{11}$
R(3C)	$OOQ+h\nu \rightarrow Q+OO$	$k_{13}=0.5\times0.983\times k_{11}$
R(3D)	$OQO+h\nu\nu \rightarrow O+OQ$	$k_{14}=0.983\times k_{11}$
R(3E)	$OOP+h\nu \rightarrow O+OP$	$k_{15}=0.5\times k_{11}$
R(3F)	$OOP+h\nu \rightarrow P+OO$	$k_{16}=0.5\times0.989\times k_{11}$
R(3G)	$OPO+h\nu \rightarrow O+OP$	$k_{17}=0.989\times k_{11}$
R4 (ozone decomposition)		
R(4A)	$OOO+O \rightarrow OO+OO$	$k_{27}=8.0\times10^{-15}$
R(4B)	$OOO+O(^1D) \rightarrow OO+O+O$	$k_{28}=0.5\times1.2\times10^{-10}$
R(4C)	$OOO+O(^1D) \rightarrow OO+OO$	$k_{29}=k_{28}$
R(4D)	$OOO+OO(^1D) \rightarrow OO+OO+O$	$k_{30}=3.8\times10^{-15}$
R(4E)	$OOO+Q \rightarrow OO+OQ$	$k_{31}=0.957\times k_{27}$
R(4F)	$OOO+Q(^1D) \rightarrow OO+O+Q$	$k_{32}=0.957\times k_{28}$
R(4G)	$OOO+Q(^1D) \rightarrow OO+OQ$	$k_{33}=k_{32}$
R(4H)	$OOO+OQ(^1\Delta) \rightarrow OO+OO+Q$	$k_{34}=0.5\times0.982\times k_{30}$
R(4I)	$OOO+OQ(^1\Delta) \rightarrow OO+OQ+O$	$k_{35}=k_{34}$
R(4J)	$OOO+P \rightarrow OO+OP$	$k_{36}=0.978\times k_{27}$
R(4K)	$OOO+P(^1D) \rightarrow OO+O+P$	$k_{37}=0.978\times k_{28}$
R(4L)	$OOO+P(^1D) \rightarrow OO+OP$	$k_{38}=k_{37}$
R(4M)	$OOO+OP(^1\Delta) \rightarrow OO+OO+P$	$k_{39}=0.5\times0.991\times k_{30}$
R(4N)	$OOO+OP(^1\Delta) \rightarrow OO+OP+O$	$k_{40}=k_{39}$
R(4O)	$OOQ+O \rightarrow OO+OQ$	$k_{41}=0.995\times k_{27}$
R(4Q)	$OOQ+O(^1D) \rightarrow OO+Q+O$	$k_{42}=0.5\times0.995\times k_{28}$
R(4P)	$OOQ+O(^1D) \rightarrow OQ+O+O$	$k_{43}=k_{42}$
R(4R)	$OOQ+O(^1D) \rightarrow OO+OQ$	$k_{44}=0.995\times k_{28}$
R(4S)	$OOQ+OO(^1\Delta) \rightarrow OO+OQ+O$	$k_{45}=0.992\times k_{30}$
R(4T)	$OOP+O \rightarrow OO+OP$	$k_{46}=0.997\times k_{27}$
R(4U)	$OOP+O(^1D) \rightarrow OO+P+O$	$k_{47}=0.5\times0.997\times k_{28}$
R(4V)	$OOP+O(^1D) \rightarrow OP+O+O$	$k_{48}=k_{47}$
R(4W)	$OOP+O(^1D) \rightarrow OO+OP$	$k_{49}=0.997\times k_{28}$
R(4X)	$OOP+OO(^1\Delta) \rightarrow OO+OP+O$	$k_{50}=0.996\times k_{30}$
R(4Y)	$OQO+O \rightarrow OQ+OO$	$k_{51}=0.995\times k_{27}$
R(4Z)	$OQO+O(^1D) \rightarrow OQ+O+O$	$k_{52}=0.995\times k_{28}$
R(4AA)	$OQO+O(^1D) \rightarrow OQ+OO$	$k_{53}=k_{52}$
R(4AB)	$OQO+OO(^1\Delta) \rightarrow OQ+OO+O$	$k_{54}=0.992\times k_{30}$
R(4AC)	$OPO+O \rightarrow OP+OO$	$k_{55}=0.997\times k_{27}$
R(4AD)	$OPO+O(^1D) \rightarrow OP+O+O$	$k_{56}=0.997\times k_{28}$
R(4AE)	$OPO+O(^1D) \rightarrow OP+OO$	$k_{57}=k_{56}$
R(4AF)	$OPO+OO(^1\Delta) \rightarrow OP+OO+O$	$k_{58}=0.996\times k_{30}$
R5 ($O(^1D)$ quenching)		
R(5A)	$O(^1D)+OO \rightarrow O+OO$	$k_{59}=4.0\times10^{-11}$
R(5B)	$Q(^1D)+OO \rightarrow Q+OO$	$k_{60}=0.962\times k_{59}$
R(5C)	$P(^1D)+OO \rightarrow P+$OO	$k_{61}=0.980\times k_{59}$
R6 [$OO(1\Delta)$ quenching]		
R(6A)	$OO(^1\Delta)+M \rightarrow OO+M$	$k_{62}=1.7\times10^{-18}$
R(6B)	$OQ(^1\Delta)+M \rightarrow OQ+M$	$k_{63}=0.986\times k_{62}$
R(6C)	$OP(^1\Delta)+M \rightarrow OP+M$	$k_{64}=0.993\times k_{62}$

close to the observed number. Possibly this is also the reason for getting lower values of δ^{18}O in samples of set 3. Considering all the sets, the contribution of surface effect in $\Delta(\delta^{13}C)$ is (on average) about 18‰ which implies lowering of δ^{18}O by about 36‰. The mass independent effect is considerably reduced when the recombination occurs on the walls of the reaction vessel since wall-induced deactivation of the vibrationally excited intermediate[6,19] is expected to obey simple mass dependence.

C. Simulation of earlier O+CO experimental data

We also reexamined the experimental data of BT (Refs. 28 and 29) in the light of KINTECUS model. Model result shows that expected δ^{18}O value of the CO_2 varies from −76.1 to −62.8 whereas the respective variation in δ^{17}O is from −31.2 to −30.6‰ (Table VII). The enrichment in ^{18}O of CO_2 varies from 78.4 to 127.7 which are slightly larger than that of set 4 samples even though the experimental condi-

TABLE VII. Results of model simulation of Bhattacharya-Thiemens data [O_2 and CO mixture was photolysed with UV lamp (case 1 to 8 Hg lamp and 9, 10 Kr lamp)] (δ values are in ‰ relative to VSMOW). Enrichments defined as the difference of observed value from the model prediction are also shown.

Sample No.	O_2 initial amount (μmol)	CO/O_2 ratio	Exposure time (min)	Amount of CO_2 produced (μmol)	CO_2 composition		Model prediction		Enrichment in CO_2	
					$\delta^{18}O$	$\delta^{17}O$	$\delta^{18}O$	$\delta^{17}O$	$\Delta(\delta^{18}O)$	$\Delta(\delta^{17}O)$
1	185	423	1020	16	12.2	25.5	−66.8	−30.9	79.0	56.4
2	353	246	2325	58	38.2	39.2	−73.3	−31.0	111.5	70.2
3	282	298	960	50	33.1	33.0	−65.1	−30.9	98.2	63.9
4	265	422	1060	58	37.4	36.3	−63.8	−30.6	101.2	66.9
5	260	345	1330	63	29.5	29.4	−67.6	−30.9	97.1	60.3
6	254	353	1020	20	13.2	18.6	−65.2	−30.9	78.4	49.5
7	245	229	1320	23	10.1	14.3	−72.6	−31.4	82.7	45.7
8	630	178	1110	35	16.3	24.0	−62.8	−30.6	79.1	54.6
9	253	343	1065	41	60.6	59.3	−65.9	−30.8	126.5	90.1
10	250	314	2660	49	51.6	55.1	−76.1	−31.2	127.7	86.3

[a]The initial oxygen isotopic composition of O_2 and CO was $\delta^{18}O=18.0$ and $\delta^{17}O$ and $\delta^{18}O=16.1$ and $\delta^{17}O=8.4$, respectively (in ‰ relative to VSMOW).

tions were nearly the same. Data from both sets of experiments are plotted in Fig. 6. A small difference in enrichment could be due to low CO/O_2 ratio (6–53) in set 4 as compared to that of BT experiments where this ratio was much higher (178–423).

The enrichments in $^{17}O/^{16}O$ and $^{18}O/^{16}O$ of CO_2 show good correlations (Fig. 7). The best-fit lines have slopes of 0.87, 0.81, and 0.74 for 70 cc (sets 1 and 2), 5 l (Sets 3 and 4), and BT experiments, respectively.

V. IMPLICATIONS

The present set of experiments confirms the earlier results of BT and establishes the level of anomalous oxygen isotope enrichments in product CO_2 arising from O+CO reaction. Marcus and co-workers[13–19] proposed and developed a phenomenological theory, which has been fairly successful to explain many features of the unusual isotope effect associated with ozone formation processes. This theory is based on restrictions of symmetry on the process of energy sharing among the rotational/vibrational states of the ozone isotopomers and their influence on the rate of stabilization of a given ozone isotopomer. They introduced a symmetry driven parameter η, which denotes a small relative deviation from the statistical density of states for symmetric isotopomers (density of states is reduced by a factor of η) compared with asymmetric isotopomers. As mentioned by Marcus,[19] the η effect could arise from both intramolecular and intermolecular energy transfer properties of a molecule.

We apply the same arguments to explain the enrichment in CO_2 case. Collision of Q and CO or O and CQ involves formation of a rovibrationally excited OCQ^* complex which must redistribute its excess energy among the available vibrational-rotational modes to become stable OCQ. The process of energy randomization depends on the strength of vibration-rotation and vibration-vibration couplings as well as the number of pathways. Asymmetric OCQ^* has a com-

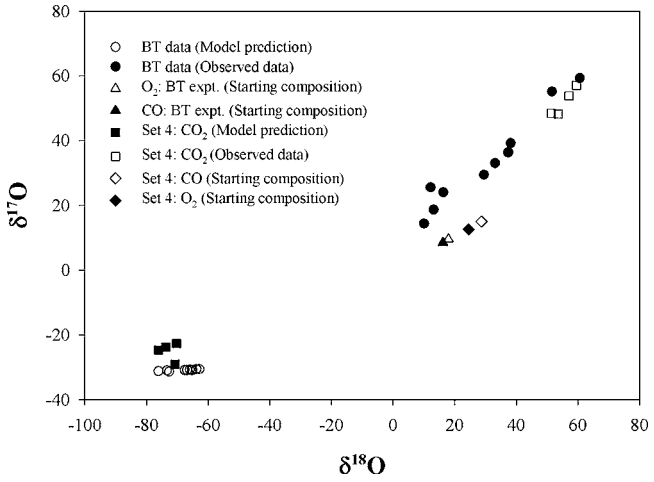

FIG. 6. A three isotope plot showing the oxygen isotopic composition of the product CO_2 in case of set 4 and BT experiments. The average enrichment observed in BT experiments is $\delta^{18}O=98.1$ and $\delta^{17}O=64.4$ whereas in set 4 (present experiment) the values are $\delta^{18}O=128.1$ and $\delta^{17}O=76.9$. Lower enrichment observed in BT case could be due to a larger amount of the product CO_2 as compared to that of set 4.

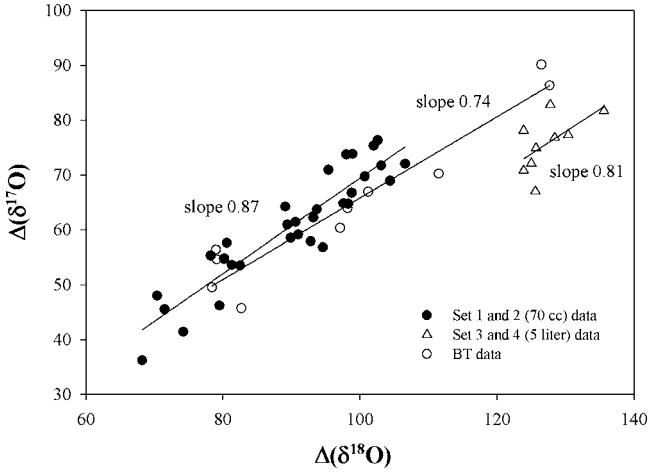

FIG. 7. Three isotope plot showing correlation between enrichments in ^{18}O and ^{17}O of the CO_2 produced from O+CO reaction. Enrichments in sets 1 and 2 fall on a line with a slope 0.87 (similar to the value in case of ozone formation by $O+O_2$ reaction). The enrichment varies from 70‰ to 136‰ and 41‰ to 83‰ in ^{18}O and ^{17}O. For sets 3 and 4, CO_2 has higher enrichments (probably due to mass dependent fractionation) compared to that in sets 1 and 2 but the slope is similar (~0.8).

paratively stronger coupling due to the presence of anharmonic vibration-vibration and Coriolis vibration-rotation coupling terms compared to the symmetric species OCO^*. So it is relatively easier for OCQ^* to redistribute the excess energy among its modes as compared to OCO^*. The faster randomization yields a longer lifetime of that particular complex. This results in a higher formation rate for OCQ type. The intramolecular η effect thus depends on the symmetry type of isotopologues.

Gas phase chemical reaction rates are strongly dependent on the intermolecular collisional energy transfer. In the intermolecular collisional energy transfer, energy is transferred between the excited CO_2^* and a bath gas molecule in discrete steps of ΔE per collision. The energetic molecule with energy less than ΔE above the threshold leads to a deactivated molecule. Energy transfer from rotation to translation ($R \rightarrow T$) and vibration to rotation ($V \rightarrow R$) is more efficient than vibration to vibration ($V \rightarrow V$) and vibration to translation ($V \rightarrow T$). Energy transfer rate depends on the number of rotational and vibrational states present in CO_2^* near the dissociation limit and on the coupling between them. The density of states in OCQ^* is twice more than the symmetric OCO. Therefore, the transfer of excess energy is more efficient which leads to a higher rate of formation of OCQ. The formation rate also depends on amount of energy transferred per collision (ΔE). If ΔE is small a weak collision is sufficient for energy transfer. Since ΔE is smaller for OCQ^* (compared to OCO) randomization is faster and the rate of formation of OCQ is higher. Therefore, both the intramolecular energy randomization and intermolecular energy transfers lead to higher rate of formation of asymmetric molecules (i.e. heavy isotopomers). Since the symmetry is independent of mass, the enrichment in CO_2 shows a non-mass dependent effect.

A. Comparison of enrichments in CO_2 and O_3

Ozone has two isotopomers corresponding to mass 50: $^{16}O^{16}O^{18}O$ (asymmetric) and $^{16}O^{18}O^{16}O$ (symmetric). It has been seen that the enrichment in ozone has contribution from both asymmetric and symmetric species but the contributions are different. For example, if the total enrichment in ozone ($\delta^{50}O_3$) is 131‰, the enrichments in asymmetric and symmetric species are 151‰ and 92‰, respectively. In contrast to this, enrichment in CO_2 is only due to asymmetric species ($^{16}O^{12}C^{18}O$). It has no heavy symmetric species. So for comparing enrichments in O_3 and CO_2, we should consider only asymmetric species of ozone ($^{16}O^{16}O^{18}O$).

At a pressure of about ~30 torr a total enrichment of about 130‰ in ozone (both species) is observed corresponding to an enrichment of ~150‰ in asymmetric ozone. Our experiments show that enrichment in CO_2 varies from ~124‰ to 136‰ in the CO pressure range of about 14–28 torr. For comparison, only sets 3 and 4 data are to be considered because other data show a relatively lower enrichment due to the surface effect (discussed above). Therefore, the average enrichment in CO_2 (~135‰) is less than that of ozone (~150‰) by about 15%.

We may speculate about the reason for ~15% lower enrichment in CO_2. This could be due to the presence of relatively larger density of states (ρ) in CO_2 near the threshold of dissociation. The magnitude of ρ at threshold depends on the dissociation energy of the molecule. CO_2 has relatively higher dissociation energy of about 5.5 eV compared to O_3 (~1.1 eV); so the value of ρ is comparatively higher for CO_2 than O_3. The enrichment is expected to be a function of $\Delta\rho/\rho$ where $\Delta\rho$ is the difference between the density of states of asymmetric and symmetric species. A smaller value of this ratio means less discrimination and the molecule is "less apt to show nonstatistical behavior."[19] Since the ratio $\Delta\rho/\rho$ is less in CO_2, it has lower enrichment.

There is another way to look at the effect following Bates.[10,11] It is known that in a coupled oscillator the transfer of energy between the two oscillators occurs with a frequency, which is the difference in the two normal frequencies or so-called "beat frequency." Higher the beat frequency faster is the energy transfer and consequent randomization. In molecules, energy gets transferred from one mode to the other in a similar way. The asymmetric and symmetric stretch mode frequencies in O_3 are 1104 and 1039 cm^{-1} and in CO_2 they are 2439 and 1388 cm^{-1}. The beat frequency ($\nu_1 - \nu_2$) in CO_2 is 961 cm^{-1} which is higher than that of O_3 (65 cm^{-1}). Therefore, the flow of energy within the modes is comparatively faster in case of CO_2, which results in less discrimination.

B. Investigation of effect of nuclear spin on O+CO reaction

It is interesting to investigate the effect of nuclear spin on the reaction $O(^3P)+CO(^1\Sigma^+) \leftrightarrow CO_2^*(^3B_2) \rightarrow CO_2(^1\Sigma_g^+)$. The overall reaction is spin forbidden. The perturbation produced by the spin-orbit coupling in the molecule can, however, make it go. It is possible that nuclear spin can play a role in the triplet-singlet transition part of the reaction as a result of which the rate of formation of CO_2 containing ^{17}O and ^{13}C may be enhanced since ^{17}O has spin of $\frac{5}{2}$ and ^{13}C has of $\frac{1}{2}$. However, our experiments do not show any unusual enhancement which can be ascribed to the spin effect. The reason for this becomes clear as we outline various steps of the reaction as follows. The collision of a triplet O atom with a singlet CO molecule results in the formation of an electronically vibrationally excited CO_2^* in a triplet state ($^3B_2$). To become stable, it has to give away its excess energy through a series of collisions with the surrounding molecules. While doing so it steps down the ladder of vibrational levels ultimately reaching the lowest vibrational level of the same electronic state ($^3B_2$). Transition from this triplet state to the singlet ground state by photon (radiation) emission is forbidden. However, this transition can occur in the presence of a spin-orbit coupling in the following way. According to Clyne and Thrush,[44] CO_2^* undergoes a radiative transition from the triplet state ($^3B_2$) to a *low-lying triplet state* followed by radiationless transition to the singlet ground state ($^1\Sigma_g^+$). The reversal of spin occurs in the latter step due to spin-orbit coupling. Since all molecules in this state are destined to make the transition (aided by either electron spin or nuclear spin) there is no isotope selection in this step.

VI. CONCLUSION

A set of experiments were carried out to study oxygen isotope fractionation in CO_2 formed by O+CO reaction. The expected isotopic composition of the product CO_2 was computed using a commercially available model of chemical reaction simulation (KINTECUS) incorporating standard mass dependent reaction rate constants. The isotopic composition of the product CO_2 is found to be anomalously enriched in heavy oxygen isotopes relative to that expected based on the simulation. The enrichment in heavy oxygen isotopes of CO_2 varies from 70‰ to 136‰ and 41‰ to 83‰ in ^{18}O and ^{17}O, respectively. The enrichment is not dependent on the isotopic composition of O atom used for the reaction since it is nearly the same irrespective of the sources from which it is produced. The level of enrichment seen in the CO_2 produced by O+CO reaction is in general similar to that observed earlier in case of O_3 produced by $O+O_2$ reaction. Since both these reactions involve symmetric and asymmetric product molecules ($^{16}O^{12}C^{16}O$ and $^{16}O^{12}C^{18}O$ in case of CO_2 and $^{16}O^{16}O^{16}O$ and $^{16}O^{16}O^{18}O$ in case of O_3) the mechanism proposed for explaining the isotopic enrichment in ozone by Marcus and co-workers may be applicable for CO_2. Small difference ($\sim$15%) between the two cases (lower enrichment in case of CO_2) can be explained by a higher state density in case of CO_2 resulting in less deviation from statistical abundances.

It is interesting to note a change in carbon isotopic composition of the product CO_2 from the initial CO defined as $\Delta(\delta^{13}C)$. The value of $\Delta(\delta^{13}C)$ varies from -14.6‰ to 3.8‰ and the increase correlates with decrease in CO pressure. Negative values of $\Delta(\delta^{13}C)$ obtained at high pressure of CO or done in bigger chamber suggests that if O+CO reaction occurs mainly in gas phase there is preference for lighter carbon isotope. At lower pressures, surface mediated stabilization assumes importance which makes $\Delta(\delta^{13}C)$ value positive indicating preference for heavy isotope. No anomalous enrichment is observed in ^{13}C of CO_2 as carbon being a central atom does not participate in the symmetry related part of the fractionation process.

[1] K. Mauersberger, Geophys. Res. Lett. **8**, 935 (1981).
[2] K. Mauersberger, Geophys. Res. Lett. **14**, 80 (1987).
[3] K. Mauersberger, P. Lammerzahl, and D. Krankowsky, Geophys. Res. Lett. **28**, 3155 (2001).
[4] M. H. Thiemens and J. E. Heidenreich III, Science **219**, 1073 (1983).
[5] M. H. Thiemens and T. Jackson, Geophys. Res. Lett. **14**, 624 (1987).
[6] J. E. Heidenreich III and M. H. Thiemens, J. Chem. Phys. **84**, 2129 (1986).
[7] M. H. Thiemens and T. Jackson, Geophys. Res. Lett. **15**, 639 (1988).
[8] J. Morton, J. Barnes, B. Schueler, and K. Mauersberger, J. Geophys. Res. **95**, 901 (1990).
[9] J. A. Kaye and D. F. Strobel, J. Geophys. Res. **88**, 8447 (1983).
[10] D. R. Bates, J. Chem. Phys. **93**, 2158 (1990).
[11] D. R. Bates, J. Chem. Phys. **93**, 8739 (1990).
[12] K. S. Griffith and G. I. Gellene, J. Chem. Phys. **96**, 4403 (1992).
[13] B. C. Hathorn and R. A. Marcus, J. Chem. Phys. **111**, 4087 (1999).
[14] B. C. Hathorn and R. A. Marcus, J. Chem. Phys. **113**, 9497 (2000).
[15] Y. Q. Gao and R. A. Marcus, Science **293**, 259 (2001).
[16] B. C. Hathorn and R. A. Marcus, J. Phys. Chem. A **105**, 2612 (2001).
[17] R. A. Marcus and Y. Q. Gao, J. Chem. Phys. **114**, 9807 (2001).
[18] Y. Q. Gao and R. A. Marcus, J. Chem. Phys. **116**, 137 (2002).
[19] R. A. Marcus, J. Chem. Phys. **121**, 8201 (2004).
[20] D. Babikov, B. K. Kendrick, R. B. Walker, R. T. Pack, P. Fleurat-Lessard, and R. Schinke, J. Chem. Phys. **118**, 6298 (2003).
[21] D. Babikov, B. K. Kendrick, R. B. Walker, R. T. Pack, P. Fleurat-Lessard, and R. Schinke, J. Chem. Phys. **119**, 2577 (2003).
[22] D. Babikov, B. K. Kendrick, R. B. Walker, R. Schinke, and R. T. Pack, Chem. Phys. Lett. **372**, 686 (2003).
[23] M. V. Ivanov, S. Y. Grebenshchikov, and R. Schinke, J. Chem. Phys. **120**, 10015 (2004).
[24] S. M. Anderson, D. Hulsebusch, and K. Mauersberger, J. Chem. Phys. **107**, 5385 (1997).
[25] K. Mauersberger, B. Erbacher, D. Krankowsky, J. Gunther, and R. Nickel, Science **283**, 370 (1999).
[26] C. Janssen, J. Guenther, D. Krankowsky, and K. Mauersberger, J. Chem. Phys. **111**, 7179 (1999).
[27] C. Janssen, J. Guenther, K. Mauersberger, and D. Krankowsky, Phys. Chem. Chem. Phys. **3**, 4718 (2001).
[28] S. K. Bhattacharya and M. H. Thiemens, Z. Naturforsch., A: Phys. Sci. **44a**, 435 (1989).
[29] S. K. Bhattacharya and M. H. Thiemens, Z. Naturforsch., A: Phys. Sci. **44a**, 811 (1989).
[30] S. K. Bhattacharya, J. Savarino and M. H. Thiemens, Geophys. Res. Lett. **27**, 1459 (2000).
[31] S. S. Assonov and C. A. M. Brenninkmeijer, Rapid Commun. Mass Spectrom. **15**, 2426 (2001).
[32] J. C. Ianni, KINTECUS, Vast Technologies Development, Inc., Kintecus License Division 26, Willowbrook Ave, Lansdowne, Pa 19050, electronic mail: jci10@hotmail.com.
[33] S. Chakraborty and S. K. Bhattacharya, J. Chem. Phys. **118**, 2164 (2003).
[34] S. M. Anderson, F. S. Klein, and F. Kaufman, J. Chem. Phys. **83**, 1648 (1985).
[35] W. B. DeMore, S. P. Sander, D. M. Golden, R. F. Hampson, M. J. Kurylo, C. J. Howard, A. R. Ravishankara, C. E. Kolb, and M. J. Molina, Jet Propul. Lab, Pubilcation No. 97–4Pasadena, California, 1997).
[36] M. G. Sheppard and R. B. Walker, J. Chem. Phys. **78**, 7191 (1983).
[37] C. Janssen, J. Geophys. Res. **110**, D08308 (2005).
[38] J. Wen and M. H. Thiemens, J. Geophys. Res. **96**, 10911 (1991).
[39] S. Jaffe and F. S. Klein, Trans. Faraday Soc. **62**, 3135 (1966).
[40] T. G. Slanger, B. J. Wood, and G. Black, J. Chem. Phys. **57**, 233 (1972).
[41] Y. L. Yung and W. B. DeMore, *Photochemistry of Planetary Atmospheres* (Oxford University Press, Oxford, 1999).
[42] R. Atkinson, D. L. Baulch, R. A. Cox, R. F. J. Hampson, J. A. Kerr, M. J. Rossi, and J. Troe, Atmos. Environ. **30**, 1125 (1996).
[43] S. Halas, T. Durakiewicz, and P. Mackiewicz, Surf. Sci. **555**, 43 (2004).
[44] M. A. A. Clyne and B. A. Thrush, Proc. R. Soc. London, Ser. A **269**, 404 (1962).